PAPER

A fast response miniature probe for wet steam flow field measurements

IOP Publishing Measurement Science and Technology
Meas. Sci. Technol. **27** (2016) 125901 (17pp) doi:10.1088/0957-0233/27/12/125901

A fast response miniature probe for wet steam flow field measurements

Ilias Bosdas[1,3], Michel Mansour[1], Anestis I Kalfas[2] and Reza S Abhari[1]

[1] Department of Mechanical and Process Engineering, Laboratory for Energy Conversion, ETH Zurich, Zurich, Switzerland
[2] Department of Mechanical Engineering, Aristotle University of Thessaloniki, Thessaloniki, Greece

E-mail: ibosdas@ethz.ch

Received 20 January 2016, revised 19 September 2016
Accepted for publication 20 September 2016
Published 14 October 2016

Abstract

Modern steam turbines require operational flexibility due to renewable energies' increasing share of the electrical grid. Additionally, the continuous increase in energy demand necessitates efficient design of the steam turbines as well as power output augmentation. The long turbine rotor blades at the machines' last stages are prone to mechanical vibrations and as a consequence time-resolved experimental data under wet steam conditions are essential for the development of large-scale low-pressure steam turbines. This paper presents a novel fast response miniature heated probe for unsteady wet steam flow field measurements. The probe has a tip diameter of 2.5 mm, and a miniature heater cartridge ensures uncontaminated pressure taps from condensed water. The probe is capable of providing the unsteady flow angles, total and static pressure as well as the flow Mach number. The operating principle and calibration procedure are described in the current work and a detailed uncertainty analysis demonstrates the capability of the new probe to perform accurate flow field measurements under wet steam conditions. In order to exclude any data possibly corrupted by droplets' impact or evaporation from the heating process, a filtering algorithm was developed and implemented in the post-processing phase of the measured data. In the last part of this paper the probe is used in an experimental steam turbine test facility and measurements are conducted at the inlet and exit of the last stage with an average wetness mass fraction of 8.0%.

Keywords: time resolved measurements, unsteady flow, wet steam, steam turbine, probe

(Some figures may appear in colour only in the online journal)

Nomenclature

P, p	Pressure (Pa)
T	Temperature (°C)
Cpt	total pressure coefficient (-)
K	aerodynamic coefficient (-)
V	velocity (m s^{-1})
U	voltage (volts)
G	transfer function
S	Laplace complex angular frequency
l	length (m)
f	frequency (kHz)
R	Radius (mm)
Ma	Mach number (-)

Greek

φ	flow yaw angle (°)
γ	flow pitch angle (°)
ζ	damping
σ	standard deviation
ω	frequency (rad s^{-1})
a	polynomial coefficient
k	adiabatic gas constant

[3] Author to whom any correspondence should be addressed.

Abbreviations

5HP	pneumatic 5-hole probe (Cobra shape)
FRAP-HTH	high temperature, fast response aerodynamic heated probe
MHPS	Mitsubishi Hitachi power systems
RMS	root mean square
PLA	phase lock data
GEP	Gaussian error propagation
LP	Low pressure

Subscripts

sat	saturation
t, tot	total
s, stat	static
rel	relative
ref	reference
dyn	dynamic
heater	heater location
tip	probe tip location (sensors' region)
n	natural
D	probe diameter
e	excitation
c	calibration
m	measurements
R	reference
M	model
T	traversing system
avg	time averaged value of flow quantity

Superscripts

~	time resolved data (phase locked)
–	time averaged data (mean value)
'	random part of pressure signal
i,j	polynomial order

1. Introduction

Steam turbines are widely used in power generation and they provide the world with more than 60% of its entire generated electrical power. However due to the increasing share of renewable power within the existing electrical power network, steam turbines require operational flexibility [1]. As a consequence, part load operating time has increased accordingly. The power output of modern low-pressure steam turbines has increased resulting to the latest development of blade lengths up to 60 inches [2, 3]. This results in a challenging design of the turbine blades with relative supersonic flow speeds at the blade tip region and a blade tip circumferential speed reaching up to 750 m s^{-1}. The flow environment at part load conditions becomes even more challenging for the last stages due to high wetness mass fractions (up to 10%) and water droplets sizes that range from few micrometers up to 100 μm or even 400 μm in diameter [4]. Thus, the aerodynamic design of the last stages of steam turbines has a direct impact on their mechanical integrity since the unsteady pressure fluctuations, enhanced at part load conditions, result in mechanical vibrations and high cycle fatigue reducing the lifetime of the rotating components.

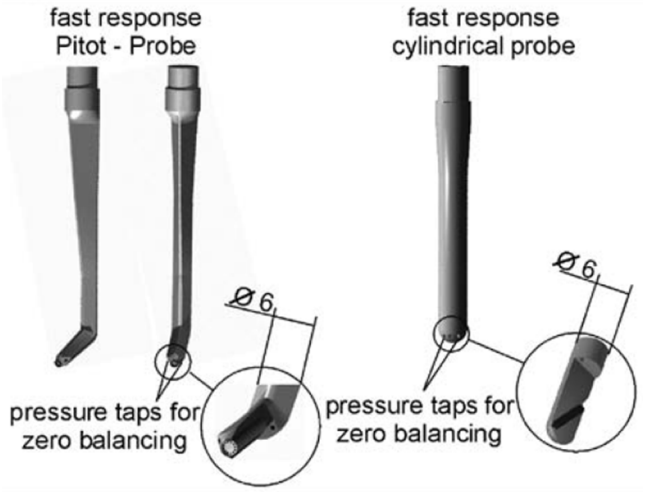

Figure 1. Single sensor fast response probe by Gerschütz *et al* [9]. Reproduced with permission. Copyright Sage Publications 2005.

Traditional pneumatic probes with air purging systems are commonly used in the wet steam environment [5, 6]. However the low measurement bandwidth, due to the long pressure lines, does not allow for the study of the unsteady flow field between the stator and rotor blades, which affect the aeromechanical performance of the axial machines [7]. As a consequence the need for time resolved measurements in the last stages of LP steam turbines is high. So far, researchers have only performed unsteady pressure measurements with flush mounted pressure sensors on the stators or the outer walls of the flowpath of LP steam turbines [3, 8]. With this type of measurements the only flow information that can be obtained is the unsteady static pressure, which does not enable the identification and characterization of the unsteady secondary flow features responsible for the rotor blades' unsteady pressure loading.

According to the author's knowledge, there is only one attempt reported in the open literature about measuring unsteady aerodynamic properties inside the wet steam environment using a fast response probe and this is by Gerschütz *et al* [9]. As shown in figure 1, Gerschütz *et al* manufactured two fast response total pressure probes for measurements in wet steam. Both consist of two pneumatic pressure taps for balancing in flow direction and one total pressure tap equipped with a Kulite® sensor for unsteady total pressure measurements. It should be mentioned that the probes are not heated and therefore they are prone to water contamination and clogging. The probes can operate at temperatures up to 275 °C and have a tip diameter of 6 mm. In their results, Gerschütz *et al* provide a detailed FFT analysis at the inlet and exit of the last stage, as well as downstream of the stator in a downscale steam turbine test facility during windage. The experimental data show that the unsteady pressure fluctuations increase when the flow is reduced below 25% of design mass flow and that the excitations are strongest near the outer casing. In addition, their analysis showed that high-amplitude fluctuations occur at distinct frequencies and that these rotate in the circumferential direction at a fraction of the rotor speed. In addition, the

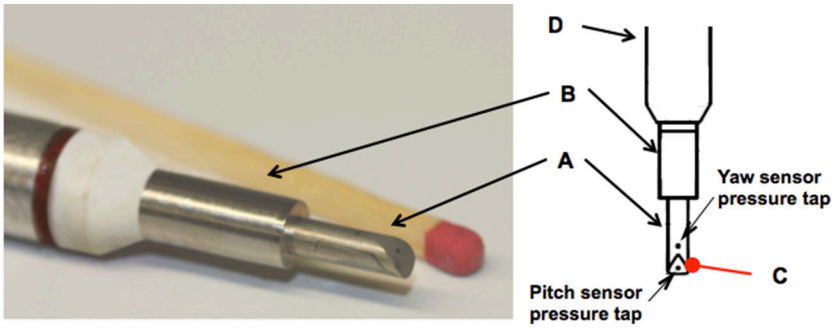

Figure 2. FRAP-HT Heated probe tip schematic.

current probes provide the unsteady total pressure field in areas where the flow field can be considered quasi two-dimensional. As a consequence no other unsteady information such as flow angles, static pressure and Mach number can be measured.

This paper presents the design, development and manufacture of a novel fast response heated probe (FRAP-HTH) for time resolved measurements under wet steam conditions. Measurements were conducted with the new probe at the last stages of MHPS' low-pressure steam turbine test facility in Hitachi in Japan. The FRAP-HTH measurements enable the identification of secondary flow structures, which are strongly related with the aerodynamic losses and the accelerated life consumption of the rotating parts. Additional information on the current measurement campaign can be found in [10–12].

2. Probe description

The design and operation of the new fast-response probe for steam measurements are based on the developments made over the past two decades at the Laboratory for Energy Conversion at ETH Zurich [13–17]. In particular, the new FRAP-HTH probe is an improved version of the FRAP-HT probe developed by Lenherr *et al* as presented in [16]. As shown in figure 2, the probe consists of two pressure taps, one for yaw angle sensitivity (yaw sensor pressure tap) and one for pitch angle sensitivity (pitch sensor pressure tap). It has a tip diameter of 2.5 mm and an overall length of 1.3 m and is able to access the flow path from the thick outer casing of the steam turbine. The probe utilizes two miniature piezoresistive pressure transducers that are used to measure the flow angles as well as the total and static pressure. The silicon-based piezoresistive pressure sensors operate in a Wheatstone bridge configuration with constant current and are used in a differential pressure measurement mode with a linear pressure range up to 1200 mbar. Their dimensions are length 2.2 mm by width 1.3 mm and a thickness of 0.4 mm. The sensors show full linearity at least up to 200 °C. AlSi alloy bonding pads embedded on the sensor are the interface for the electronic connection to the electronic circuit located at the tip of the probe. In order to mechanically decouple the sensor from the base substrate (probe body) and reduce mechanical stresses on the sensor membrane, a dual component room-temperature-vulcanizing

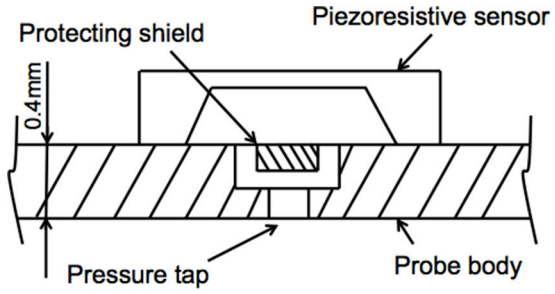

Figure 3. Schematic of the pressure tap with the protecting shield for direct droplet impact protection.

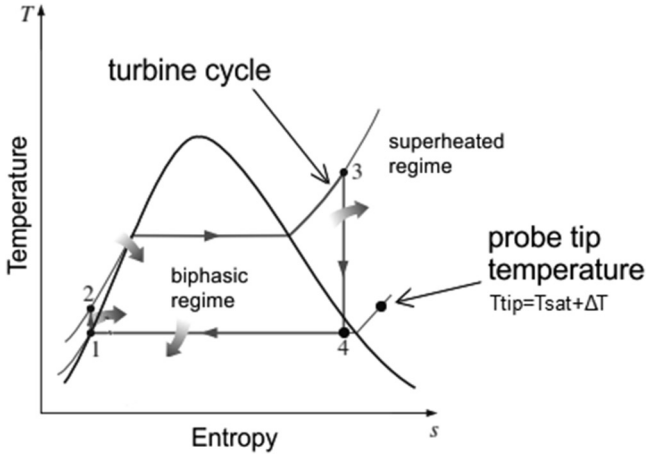

Figure 4. *T-S* diagram with steam turbine operating cycle and the respective probe tip operating temperature. Reproduced with permission from [10]. Copyright ASME 2015.

RTV silicon elastomer able to withstand temperatures up to 260 °C is used as a soft bonding agent. The probe tip is pressurized with a reference pressure that is controlled by a high precision pressure controller with an accuracy of ±0.01 mbar. In addition, the two pressure taps are equipped with a metal shield as shown in figure 3 for protecting the miniature piezoresistive sensors from direct water droplet impact.

As indicated in figure 2, the new feature of the FRAP-HTH probe is the high power density heater (B), which is installed at the probe tip (A). In order to operate the probe with unclogged pressure taps and avoid any water contamination, the tip of the probe is heated 5–10 °C above the flow saturation temperature

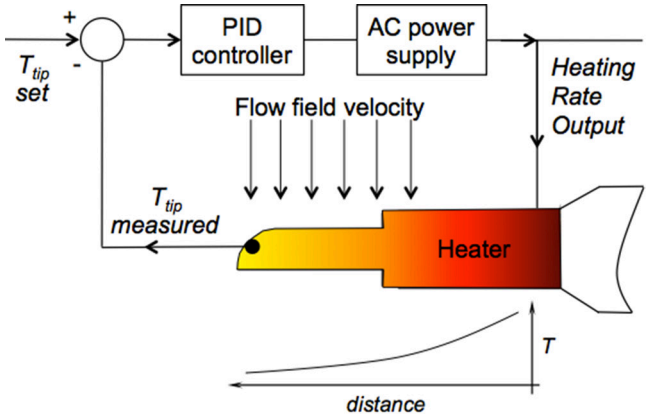

Figure 5. PID block diagram for probe's miniature heater control.

T_{sat} as shown in figure 4. The probe tip is heated through a high power density heater with a power of 61 W cm^{-2}. The heater (B) consists of a miniature heating wire installed in a double helix spiral, which is on a high thermally conductive ceramic mounted on the probe. This component has 9 mm length, an overall diameter of 4.7 mm and is installed four probe tip diameters from the tip. It is equipped with three thermocouples, which enable the temperature drop from the heater to the tip under various flow conditions to be measured experimentally. In addition, it is fed with an AC current at constant voltage and is coated with a hydrophobic coating to reduce the heat losses from the condensed water on its surface. With the current installed power, the probe was successfully operated at up to 8% wetness mass fraction, Mach number of 0.85 and flow pitch angles of up to 40°. In addition, the probe tip temperature is controlled using a closed-loop PID regulator as depicted in figure 5. The probe tip set temperature (T_{tip} set) is achieved by varying the heating power duty cycle based on the measured temperature of the piezoresistive pressure sensors located in the tip (T_{tip} measured).

3. Static calibration

The pressure sensor's working principle is the Wheatstone bridge which is fed with a constant current source of 1 mA. As shown in figure 6, the excitation voltage, *Ue* depends primarily on the membrane temperature and the signal output voltage, *U* is primarily proportional to the differential pressure across the membrane. The signal-conditioning unit placed on the rear part of the probe shaft amplifies the pressure voltage signal by a factor of 100 to enable a high signal-to-noise ratio.

The calibration procedure described by Kupferschmied *et al* in [18] is applied to derive a sensor calibration model and obtain the relationship between output voltage, pressure and temperature. For the current work, the probe was calibrated within a relative pressure range of 0 to 1050mbar and temperature range from 20 °C to 120 °C. Both ranges define a calibration matrix with corresponding voltage $U(P,T)$ and $Ue(P,T)$ as a function of pressure P and temperature T. Figure 7 shows the sensor calibration results of the FRAP-HTH, where the pressure $U(P)$ and temperature $Ue(T)$ are plotted as a function of pressure and temperature signals for the yaw pressure sensor. The pitch sensor calibration has the same curves with a small difference in sensitivity $<1\%$. This results in a mean pressure sensitivity of 3.8 mV mbar^{-1} for both sensors and a mean temperature sensitivity of 2.8 mV °C^{-1} for both sensors. Nevertheless during the measurements with the FRAP-HTH probe each sensor has its own calibration curve in order to increase the accuracy of the results to the maximum.

4. Virtual 6 sensor mode

The large flare angles present in the last stages of LP steam turbines require a special operation of the new FRAP-HTH probe. Typical tip wall flare angles range from 30° to 40°. As shown in figure 8, in order to enable measurements in such high flow pitch angles, the probe is operated in a virtual six-sensor mode. This measurement concept is an extension of the virtual 4-sensor measurement concept as described in [14, 16], which only allow flow field measurements up to approximately 35° of pitch angle due to the separation of the flow on the leeward side of the probe.

The schematic in figure 8 shows the virtual 6-sensor mode measurement concept using the current probe that is equipped with two sensors, the yaw pressure sensor and pitch pressure sensor as indicated in figure 2. The yaw pressure sensor is used to measure the actual tap pressures ($p1$, $p2$, $p3$) in three consecutive steps. This is achieved by rotating the probe along its axis at three different set angles 0°, −42°, +42° respectively. The pitch pressure sensor is used to measure the actual tap pressures $p4$, $p5$ and $p6$. The pressure $p4$ is recorded when the roll set angle is equal to 0°, whereas $p5$ and $p6$ pressures are measured at −42° and +42° roll angles respectively. Out of this procedure a set of 6 independent pressures from $p1$ to $p6$ is obtained. These pressure values are then used for the definition of the aerodynamic flow coefficients for flow yaw and pitch angles, static and total pressure as well as the absolute Mach number of the flow, as shown in table 1.

As presented in table 1, two sets of aerodynamic calibration coefficients are defined according to the actual value of the flow pitch angle relative to the probe tip. The respective flow angle validity range of the two sets of aerodynamic calibration coefficient is plotted in figure 9 for Ma = 0.7. When the measured pressure value of the yaw sensor $p1$ is larger than the pressure value of the pitch sensor $p4$, the probe is operated using the calibration coefficients defined for sector 1. For this case the aerodynamic coefficients are standard as described by [14, 16] and summarized in table 1. However when the measured value of the actual pressure $p4$ is larger than the actual pressure $p1$, the probe is operated using the second set of calibration coefficients defined for sector 2. As shown in figure 9, for the new FRAP-HTH probe shape geometry, this condition is fulfilled when the flow pitch angle is equal to 42° for the yaw incidence angle of 0° relative to the probe. The change of the calibration coefficients at the edges of the yaw angle calibration range occurs at 40° pitch.

In the post-processing code each pressure data sample is checked independently. The first set of aerodynamic coefficients is used when $p1 \geqslant p4$ (sector 1) is fulfilled in order to derive the yaw, pitch, total and static pressures and the second set of aerodynamic coefficients is used when $p1 < p4$ (sector 2).

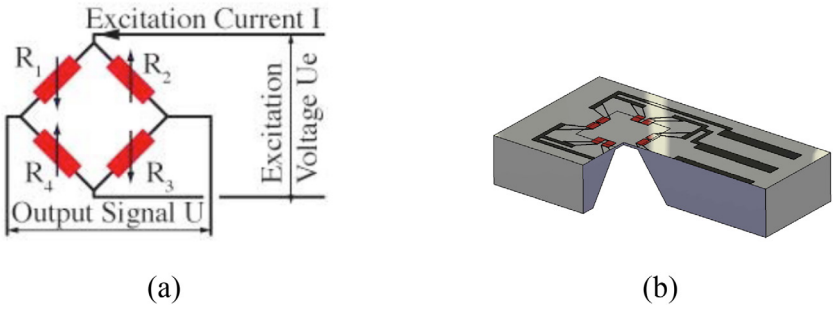

Figure 6. Wheatstone bridge schematic (a) and silicon pressure transducer cross-section at its diaphragm (b).

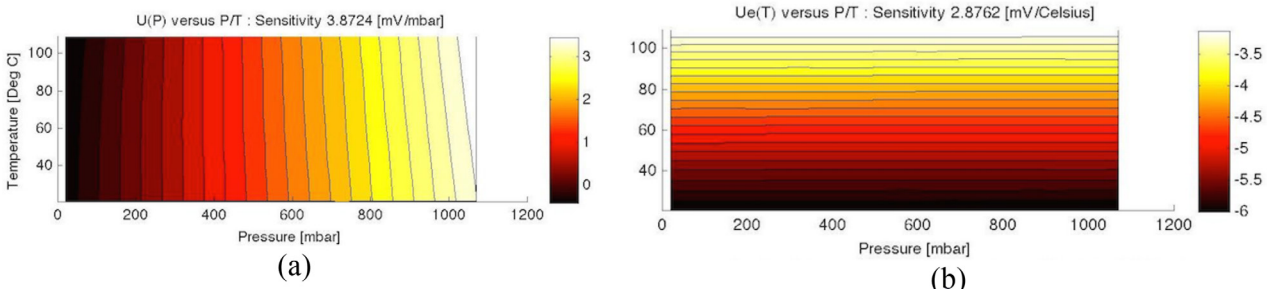

Figure 7. Calibration curve in volts for yaw sensor (a) is the *U* output and (b) is the *Ue* output.

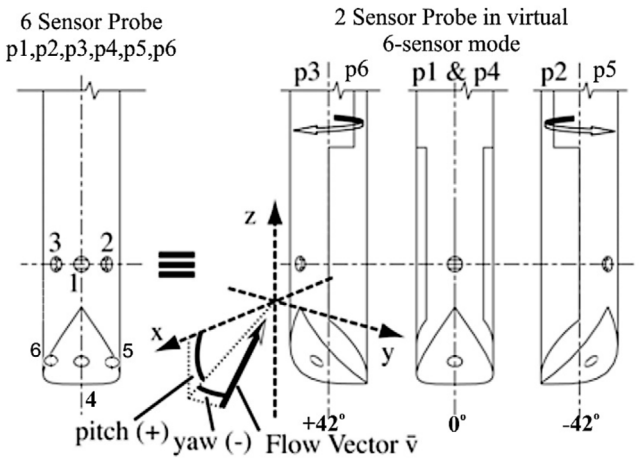

Figure 8. Virtual 6-Hole measurement concept with a 2-Hole Probe. Reproduced with permission from [10]. Copyright ASME 2015.

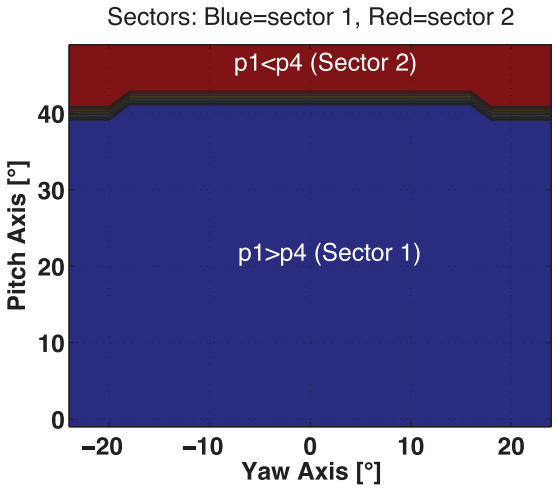

Figure 9. FRAP-HTH extended calibration section's schematic for Ma = 0.7.

Table 1. Extended aerodynamic calibration coefficients for the FRAP-HTH probe.

Sector 1 when $p_1 \geqslant p_4$ (Blue sector)	Sector 2 when $p_4 > p_1$ (Red sector)
$K_\phi = \frac{P_2 - P_3}{P_1 - \frac{(P_2+P_3)}{2}}$	$K_\phi = \frac{P_5 - P_6}{P_4 - \frac{(P_5+P_6)}{2}}$
$K_\gamma = \frac{P_1 - P_4}{P_1 - \frac{(P_2+P_3)}{2}}$	$K_\gamma = \frac{P_4 - P_1}{P_4 - \frac{(P_5+P_6)}{2}}$
$K_t = \frac{P_{tot} - P_1}{P_1 - \frac{(P_2+P_3)}{2}}$	$K_t = \frac{P_{tot} - P_4}{P_4 - \frac{(P_5+P_6)}{2}}$
$K_s = \frac{P_{tot} - P_{stat}}{P_1 - \frac{(P_2+P_3)}{2}}$	$K_s = \frac{P_{tot} - P_{stat}}{P_4 - \frac{(P_5+P_6)}{2}}$

5. Aerodynamic calibration

The FRAP-HTH probe is calibrated in freejet calibration facility of the Laboratory for Energy Conversion at ETH Zurich. The calibration facility is depicted in figure 10 with the probe installed on a three axis-traversing unit with linear motors. The facility allows all six degrees of freedom between the probe and the airflow. The jet exits from a convergent nozzle of 100 mm diameter and the probe tip is located 100 mm downstream. The head of the probe is translated relative to the fixed jet by tilting and yawing the probe shaft. The flow temperature of the jet is kept stable at 303 K (±0.3 K) via a heat exchanger located at the exit of the compressor. All flow quantities from the freejet facility are known and used for the relation of the pressures with the flow angles, total and static pressures, Mach number and flow temperature.

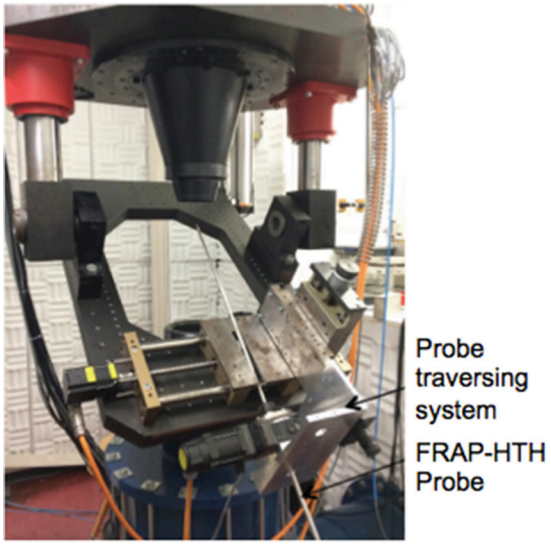

Figure 10. Extended aerodynamic probe calibration at Freejet facility.

As described in section 4 the probe is calibrated in a virtual 6-sensor mode using the 2 sets of aerodynamic calibration coefficients listed in table 1, where $K\varphi$, $K\gamma$, Kt and Ks are respectively the flow yaw angle (φ), flow pitch angle (γ) and total and static pressures (P_t and P_s) aerocalibration coefficients. As presented in table 1, the first or the second set of coefficients is chosen according to the highest pressure value measured between the yaw pressure sensor in $p1$ position and the pitch pressure sensor in $p4$ position. The polynomial curve-fit method of Gallington [19] is applied to the aerodynamic calibration data. In particular, the aerodynamic calibration model is based on a parametric approach and the flow yaw (φ) and pitch (γ) angles are derived from $K\varphi$, $K\gamma$ by an inverse calculation of the equations (1) and (2) as suggested in [20].

$$\varphi = \sum_{i=0}^{n}\sum_{j=0}^{m} a_{ij\varphi} K_{\varphi}^{i} K_{\gamma}^{j} \tag{1}$$

$$\gamma = \sum_{i=0}^{n}\sum_{j=0}^{m} a_{ij\gamma} K_{\varphi}^{i} K_{\gamma}^{j} \tag{2}$$

During the calibration procedure the flow yaw and pitch angles (φ, γ) as well as the calibration coefficients $K\varphi$, $K\gamma$ are known and the polynomial coefficients $a_{ij\varphi}$ and $a_{ij\gamma}$result from the solution of this set of linear equations using a least square approximation. The same approach is followed for the total and static pressures' polynomial coefficients using equations (3) and (4) Ks and the flow angles φ and γ are known, the polynomial coefficients a_{ijt} and a_{ijt} result from the solution of these two linear equations.

$$K_t = \sum_{i=0}^{n}\sum_{j=0}^{m} a_{ijt} \varphi^{i} \gamma^{j} \tag{3}$$

$$K_s = \sum_{i=0}^{n}\sum_{j=0}^{m} a_{ijt} \varphi^{i} \gamma^{j} \tag{4}$$

In an unknown flow field the derived calibration polynomial coefficient vectors are used for the evaluation of the unknown flow quantities from the measured set of the six pressures from $p1$ to $p6$ at given probe measurement location.

For the current work the probe was calibrated for several Mach numbers from 0.2 up to 0.8 with a step of 0.1. In the current section, the calibration results for Ma = 0.7 are presented and analyzed. Figures 11 and 12 show the resulting spatial distribution of the calibration coefficients for the first (sector 1) and second sector (sector 2) respectively, covering an overall range of ±24° in yaw angle and of −1° to +49° in pitch angle. Each figure set shows the four independent calibration coefficients as listed in table 1 and described in that section of the paper. It can be seen that for both sectors the calibration surface for the yaw angle coefficient $K\varphi$ is primarily a function of the yaw angle φ and is decoupled from the pitch flow angle γ. The same characteristic is observed for the pitch angle coefficient $K\gamma$, which is fairly well decoupled from yaw flow angle φ. In comparison to previously published FRAP-HT probes aerodynamic calibration data [14, 16], the surface pressure distribution around the probe tip of the new FRAP-HTH probe has changed due to the potential field effect of the heater (B) located close to the tip as shown in figure 2. It mainly affects the total pressure and stagnation pressure coefficient distribution in sector 1. The stagnation condition is now obtained at 25° pitch angle whereas for the standard FRAP-HT the stagnation pressure is achieved at 10° pitch angle for Ma = 0.7. In addition, the presence of the heater has the benefit to delay the separation of the boundary layer for positive pitch angle incidence, enabling a larger measurement range in positive pitch flow angles compared to the standard FRAP-HT.

The accuracies of calibration models obtained from the polynomial interpolation are provided in table 2 for Ma = 0.7. The best calibration curve fit is obtained with a polynomial order of 6 and 4 for the yaw and pitch flow angle respectively and for a polynomial order of 8 and 6 for the total and static pressure coefficients as defined in equations (1)–(4). For both sectors the models' deviations remain below ±0.25° and ±3 mbar in flow angles and pressures respectively. It is worth mentioning that the relatively high error of this particular Mach number for the total pressure in sector 1 is due to the three dimensional shape of the calibration coefficient K_t as presented in figure 11.

6. Temperature effect

The potential effect of the heater operation on the flow field around the probe tip was investigated and experimentally tested. Measurements were conducted in Freejet facility, under representative flow conditions of the last stage LP steam turbine. The representative wet steam heat transfer conditions were achieved by conducting the experiment in air under similar Nusselt number conditions. The Churchill and Bernstein relationship, which is a function of Reynolds and Prandtl number as presented in equation (5), was used to derive the representative averaged Nusselt flow conditions in air:

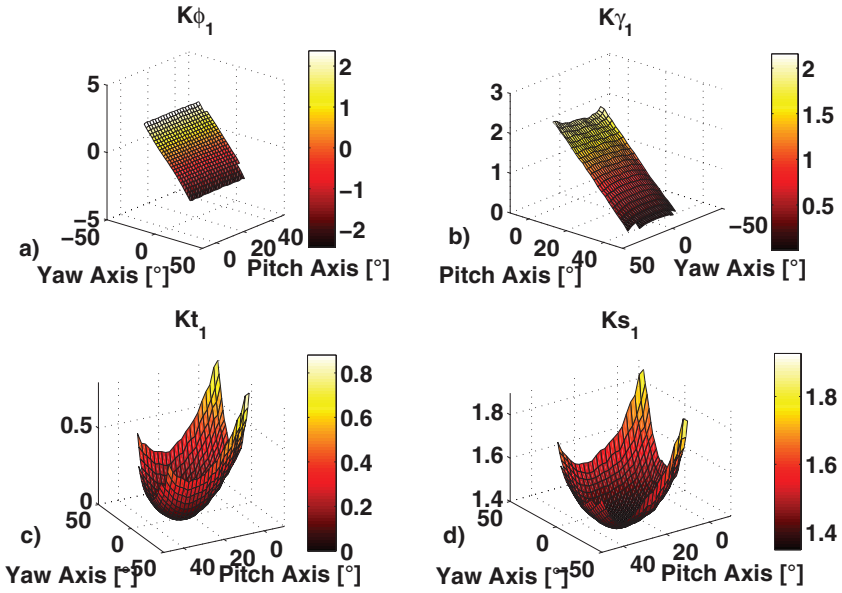

Figure 11. Aerodynamic calibration coefficients for sector 1, (a) yaw angle, (b) pitch angle, (c) total pressure, (d) static pressure.

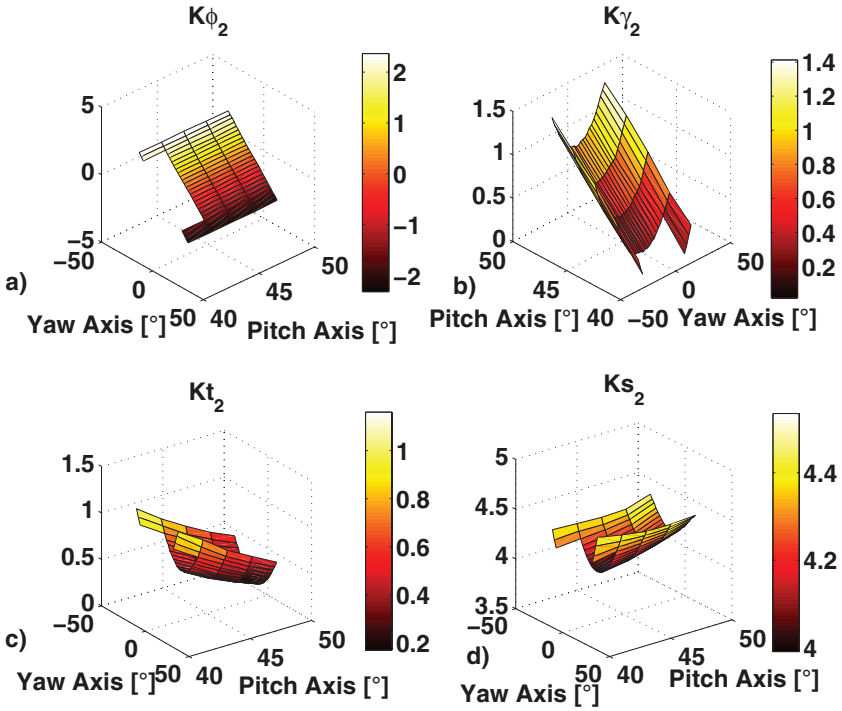

Figure 12. Aerodynamic calibration coefficients for sector 2, (a) yaw angle, (b) pitch angle, (c) total pressure, (d) static pressure.

Table 2. FRAP-HTH calibration model accuracy for Ma = 0.7 and calibration range of ±24° in Yaw and −1° < pitch < 49° in pitch.

	Probe accuracy	
Parameter:	Sector 1	Sector 2
φ	±0.15°	±0.12°
γ	±0.24°	±0.06°
P_{tot}	±490 Pa (1.3%P_{dyn})	±95 Pa (0.25%P_{dyn})
P_{stat}	±287 Pa (0.77%P_{dyn})	±244 Pa (0.65%P_{dyn})

$$\overline{Nu}_D = 0.3 + \frac{0.62\text{Re}^{1/2}\text{Pr}^{1/3}}{\left[1+\frac{0.4^{2/3}}{\text{Pr}}\right]^{1/4}}\left[1+\left(\frac{\text{Re}}{282'000}\right)^{5/8}\right]^{4/5} \quad (5)$$

The resulting average Nusselt number for the flow conditions found at the last stage of a LP steam turbine is $\overline{Nu}_D = 50$. With the Nusselt number analogy the representative flow velocity in air was calculated to be met at Ma = 0.17. Tests were conducted at Freejet facility at Ma = 0.17 for various overheat ratios and

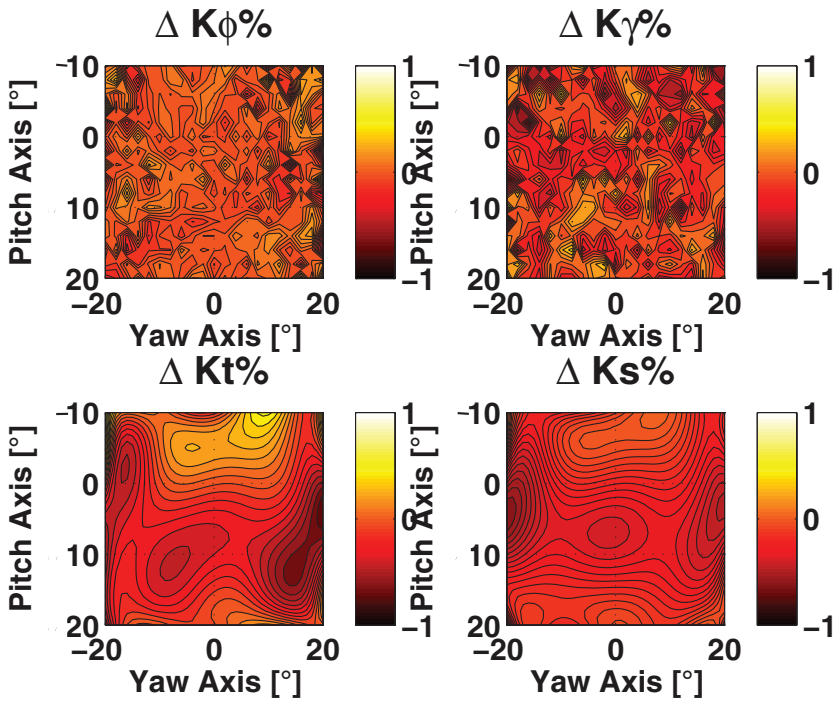

Figure 13. Effect of heater temperature at representative Nusselt flow conditions.

a wide range of yaw and pitch angles in order to identify any disturbance on the probe tip over heat on the surrounding flow.

Figure 13 shows the deviation of the four aerodynamic calibration coefficients when the heater is activated with $\Delta T = 10\,\mathrm{K}$ overheat and deactivated so that the probe tip temperature is equal to the flow air temperature. As a first observation the error for all calibration coefficients is on average below 0.5%. This practically means that the heater operation has no effect on the measured flow quantities. The streamlines of the flow at the measurement location are not distorted and therefore the flow angles as well as the total and static pressures are not affected. The resulting difference on the measured yaw and pitch angles is, on average, below 0.03° and 0.07° respectively and for total and static pressures below 10 Pa and 30 Pa respectively.

Additional assessment tests have been performed in MHPS steam turbine test facility. As described in [10, 12] the new FRAP-HTH time-averaged measurements are compared to 5HP measurements conducted on the same day at L-1 and L-0 stages' exit. The 5HP consists of a typical cobra shape probe with a tip diameter of 5 mm and is equipped with a standard air purging system. The FRAP-HTH and the 5HP measurements were performed along a single radial traverse, and it should be noted that the 5HP access hole is located at a different upstream stator clocking position compared to the FRAP-HTH. The 5HP measurements were performed with a radial spatial resolution of 33 mm. The FRAP-HTH measurements are time-averaged over 80 rotor revolutions for three rotor blade passing events. The two sets of measurements are compared at L-0 and L-1 rotor exit for the operating condition, which exhibits the most severe conditions with an average calculated wetness mass fraction of 8.0% and 3.1% at L-0 and L-1 respectively. The operating mass flow is 67*t*/*h* and the exit vacuum pressure is 8 kPa.

Figures 14(a) and (b) show the FRAP-HTH and the 5HP absolute Mach number across the blade span at L-1 and L-0 rotors' exit respectively. This flow parameter was chosen because it carries most of the uncertainty content as it is calculated at the end. In general, there is a good overall agreement between the two probes, both in the trend and in absolute values across the span. The RMS value in the absolute Mach number is 0.03 and 0.1 for L-1 and L-0 respectively. The good agreement in these flow quantities is despite the fact that both probes have different radial measurement spacing and are located at different upstream stator clocking position.

These results demonstrate the ability of the newly developed probe to provide reliable measurements at the last two stages of low pressure steam turbines under elevated wetness flow conditions and practically proves that the effect of the heater has no impact on the measured aerodynamic flow quantities.

7. Measurement bandwidth assessment

In order to assess the measurement bandwidth of the new FRAP-HTH probe, measurements were conducted in a shock tube test facility at the Laboratory for Energy Conversion. The measurement bandwidth of the probe is limited by the cavity between the silicon pressure transducer and the pressure tap of the probe. This resonant cavity effect of the probe pressure tapping has to be measured and the 3 dB amplification limit has to be found to the maximum bandwidth of the probe. The experiments were performed in air and in a second step a numerical approach to correct the results for the steam conditions was applied. The shock tube facility has 50 mm internal diameter and it is 5 m long. It consists of a high-pressure and a low-pressure section. The shock step in pressure is achieved by bursting a very thin membrane, which separates the high-pressure section from

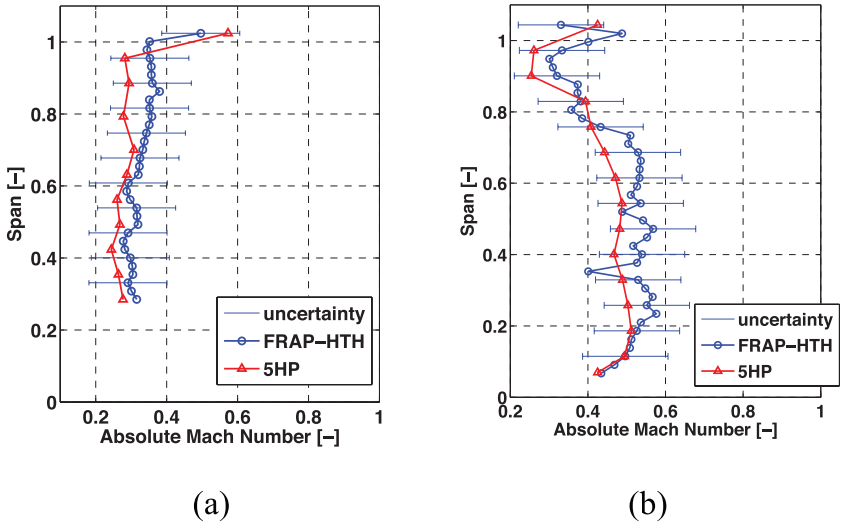

Figure 14. Absolute Mach number measured by the 5HP and FRAP-HTH probes at rotor exit of L-1 stage (a) and at the rotor exit of L-0 (b) [10]. Reproduced with permission. Copyright ASME 2015.

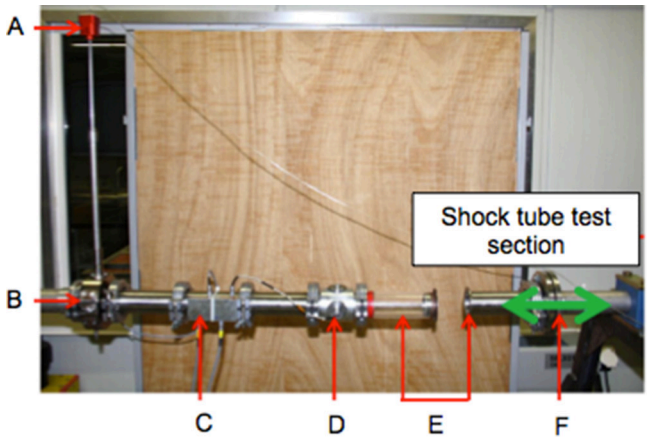

Figure 15. Shock-tube test section, (A) FRAP-HTH probe, (B) flush mounted reference probe, (C) electronics, (D) triggering sensor, (E) diagraph location, (F) high pressure section.

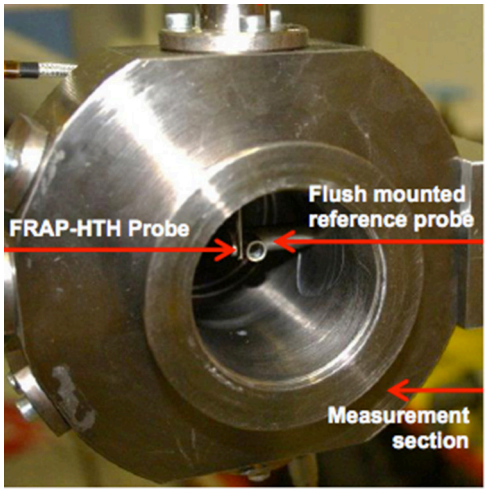

Figure 16. FRAP-HT and flush mounted reference probe.

the low pressure one. The high-pressure section is open to ambient air pressure of about 970 mbar whereas the low-pressure section is controlled by a vacuum pump. A plastic membrane is situated 0.7 m upstream of the test section and as its diaphragm breaks under a given pressure difference, a shock wave is generated and propagates with the speed of sound from the membrane location to the probe tip. This shock wave acts as a step function and excites the probe's cavity at all frequencies. Figure 15 shows the test section part of the shock tube facility. The probe A is inserted vertically and its shaft is sealed through O-rings, which are installed in the access hole. In order to generate the transfer function of the probe a second in-house built flush mounted sensor probe is installed next to the FRAP-HTH probe as depicted in figure 16. As shown in figure 15, the membrane which separates the high from low pressure section is installed at location *E*. The facility is able to produce up to 600 mbar step pressure impulses. Both probes fulfill the intrusion criteria since their diameter is less than 1/10 of the shock tube's internal diameter. The FRAP-HTH and the reference probe are shown in the measurement section of the shock tube in figure 16.

The measured step in pressure of the FRAP-HTH probe signal is compared with the reference flush mounted single sensor probe in order to derive the transfer function. The reference probe is installed on the same plane as the FRAP-HTH's pressure tap in the direction of the shock wave propagation. The signals are acquired with a PCI data acquisition 12 Bit board at 1.6 MHz for a time period of 100 ms. Both probes utilize the same type pressure transducers.

7.1. FRAP-HTH time response

The time signals for the FRAP-HTH and the reference probe from the shock tube tests are presented in figure 17. In addition the FFT results from the time signals of figure 17 are shown in figure 18. As presented in figure 18, both probes show a signal amplification at around 560 kHz which is related to the sensors' natural frequencies. This agreement of the natural frequencies is because both probes utilize the same type of piezoresistive silicon pressure transducers. In addition, there is a signal amplification associated with the FRAP-HTH's

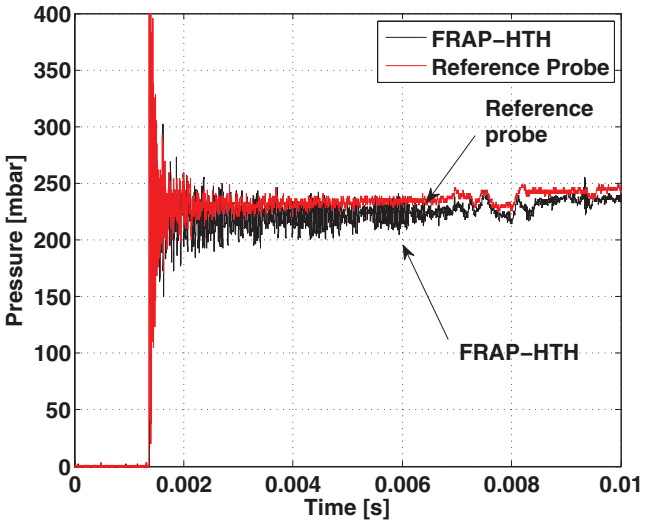

Figure 17. Time signal of FRAP-HTH and reference probe in shock tube tests.

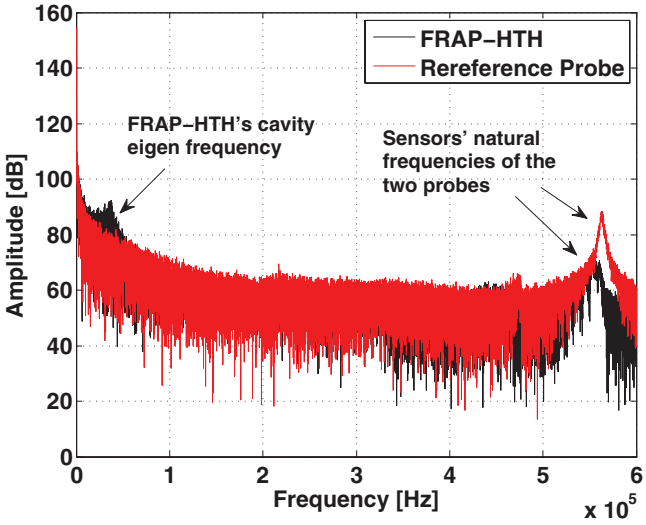

Figure 18. FFT plots of FRAP and Reference probe signals out of 10 averages.

pressure tap cavity visible at 36 kHz. In order to assess the measurement bandwidth of the FRAP-HTH, the transfer function has to be calculated out of the two signals of figure 18.

The non-parametric transfer function G_n of the FRAP-HTH probe is obtained out of the shock tube experiments with the use of the reference flush mounted sensor probe. The parametric transfer function is derived from a second order system, modeled with a polynomial fit into the non-parametric transfer function in the frequency domain. The parametric transfer function for a time continuous system can be obtained with a curve fitting approach and the mathematical problem can be reduced to a second order system using equation (6).

$$G(s) = K\frac{\omega_n^2}{s^2 + 2\zeta\omega_n s + \omega_n^2} \tag{6}$$

The values for ω_n and ζ coefficients for the parametric transfer function are obtained from the polynomial curve coefficients. The final transfer function is a result of an average out of 15

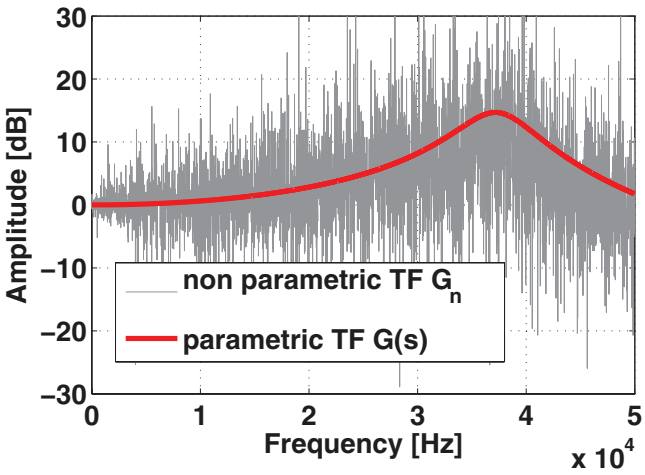

Figure 19. Comparison of parametric and non-parametric transfer function (no averaging) from a single experiment.

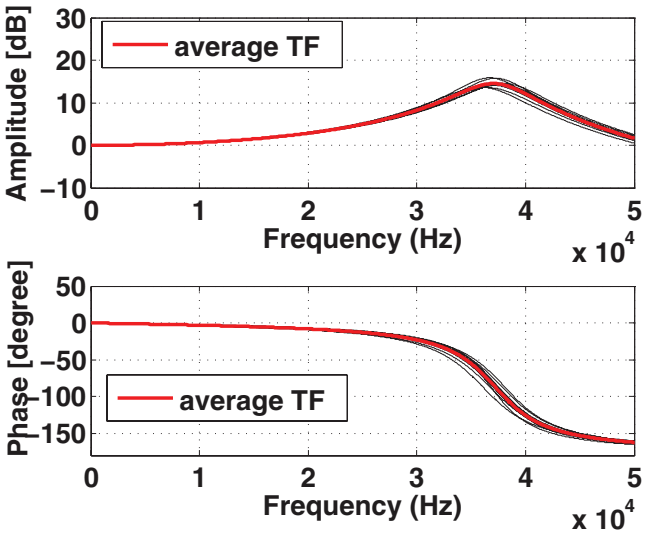

Figure 20. FRAP-HT averaged transfer function over 15 experiments in shock-tube.

tests in the shock tube facility. The main purpose for averaging the multiple non-parametric transfer functions is to reduce the noise levels, which are visible in figure 19. The averaged transfer function over 15 individual tests in the shock tube facility is shown in figure 20 up to 50 kHz. The eigenfrequency of the FRAP-HTH cavity is detected at a frequency of 36 kHz. The maximum measurement bandwidth of the FRAP-HTH is found to be at 21 kHz when the pressure signal is amplified at the value of 3 dB. In figure 20, the phase plot shows a 90° change in phase at the resonance frequency and both amplitude and phase plots represent a system with single degree of freedom.

7.2. Correction for operation in steam

Since the measurement bandwidth assessment of the FRAP-HTH probe was conducted in air, a frequency correction for measuring in steam is essential. The use of the organ pipe frequency approach with equation (7) is a good approximation because

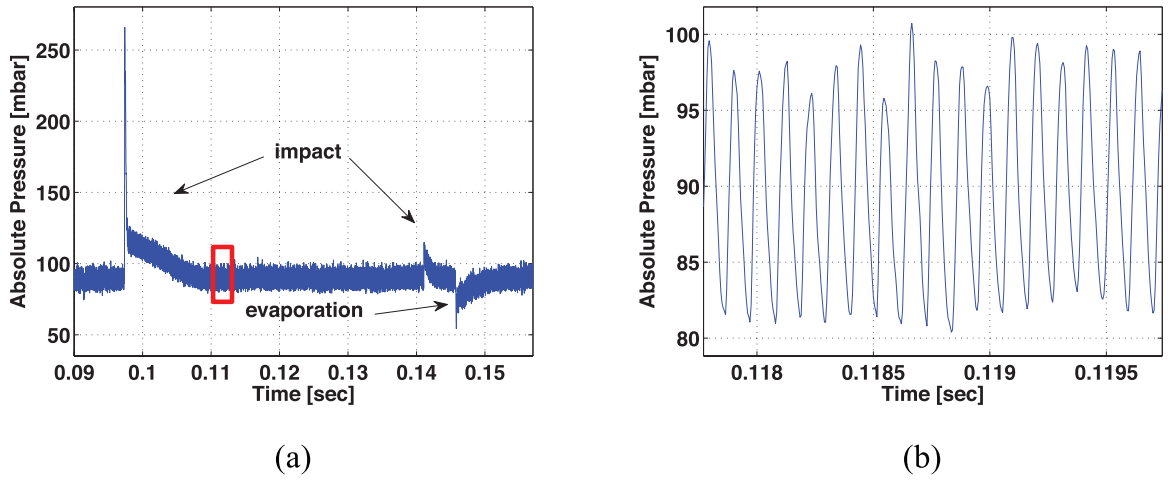

Figure 21. Probe's raw absolute pressure signal from the pitch sensor (a) and a zoomed region at the red box showing a clean part of the pressure signal with the blade passing frequency at 9.2 kHz (b).

the air and steam are both gases. According to equation (7) the natural frequency of the probe's cavity is proportional to the speed of sound and inversely proportional to the cavity length between the probe surface and the sensor' membrane.

$$f_n = \frac{\sqrt{kRT}}{4 \cdot l_{\text{cavity}}} \tag{7}$$

Therefore the change in cavity frequency from air to steam is directly proportional to the 20.5% increase in speed of sound since all other parameters remain the same:

$$\frac{\sqrt{kRT}_{\text{steam}}}{\sqrt{kRT}_{\text{air}}} = \frac{\sqrt{1.13 \cdot 461\,\text{J}\,\text{kg}^{-1}\text{K}^{-1} \cdot 330\,\text{K}}}{\sqrt{1.4 \cdot 287\text{J}\,\text{kg}^{-1}\text{K}^{-1} \cdot 296\,\text{K}}} - 1 = 20.5\%$$

As a consequence the calculated measurement bandwidth of the FRAP-HTH probe is 20.5% higher in steam than in air and is set to 25.3 kHz (3 dB limit).

8. Droplet filtering processing algorithm

As the FRAP-HTH probe operates in wet steam flows with water droplets ranging from 0.1 up to 400 μm in diameter [21], the interaction of the droplets with the pressure taps and the sensors' membrane can alter and corrupt the time-resolved pressure measurements. In particular there are two effects that can occur and result in a signal corruption. Large droplets that rest inside the pressure tap on top of the sensor shielding interface and affect the local measured pressure due to latent heat losses during the evaporation process, and the small droplets that manage to penetrate through the shielded pressure tap and impact the sensor membrane. A filtering algorithm was developed in order to filter out the portions of the raw pressure and temperature signals affected by droplets' impact or evaporation and as a result these events are discarded from the final post processed signal.

Figure 21 shows a typical set of data downstream of the last stage of a LP steam turbine at 80% span. For this operating condition the mass flow, inlet temperature and exit pressure are 67*t*/*h*, 266 °C and 8 kPa respectively. The calculated wetness mass fraction in the meridional plan is 8% and the absolute

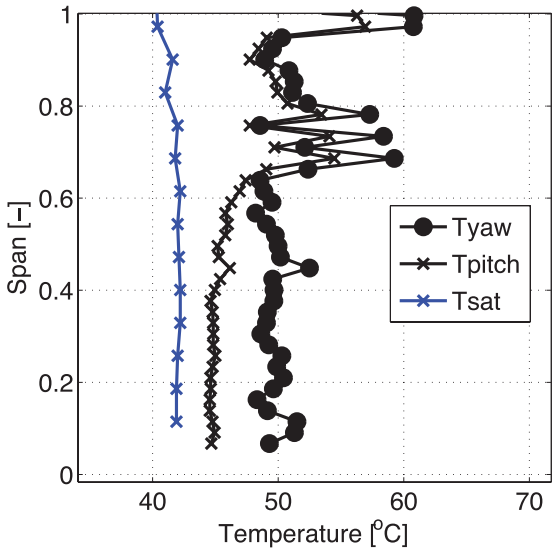

Figure 22. Actual temperature of yaw and pitch sensors along the blade span together with the measured flow saturation temperature for the exit of the last stage of LP steam turbine.

Mach number 0.5. As shown in figure 22, during theses measurements both sensors of the probe were operating above the flow saturation temperature implying that the pressure taps are clean from the condensed water. The steam temperature along the L-0 blade span remains fairly constant at 42 °C.

As presented in the figure 21, with the absolute pressure signal from the pitch sensor, the impact of small droplets can result up to an increase of 280% of the absolute measured pressure, whereas the evaporation of condensed water in the cavity results in a reduction as high as 50% of the absolute measured pressure. The evaporation of the water content in the cavity goes along with a temperature drop of the piezo-resistive sensor as shown in figure 23.

Figure 24 shows a schematic of the standard in-house data reduction code Herkules as described in [22]. The new droplet filtering subroutine is applied between Step 1 and Step 2, prior to the phasing of the measured data with respect to the turbine's rotational trigger.

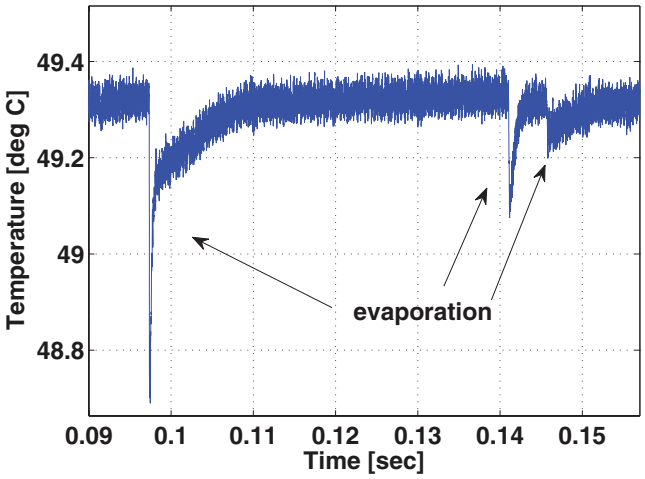

Figure 23. Probe's raw temperature signal from the pitch sensor.

As shown in figure 24, in the first step the droplet filtering code performs a phase-locked averaging on the time-resolved pressure voltage signals to quantify the mean level of the pressure signal as well as the peak-to-peak periodical pressure fluctuations triggered by the rotor blade passing frequency. The phase-locked averaged data are used to define the threshold detection boundaries of $\pm 2\sigma$ around the mean signal value, where σ is the standard deviation of the phased-locked average pressure signal. The raw turbulent data are considered as corrupted when they overshoot the $\pm 2\sigma$ limit for both impact and evaporation cases.

The case of an evaporation process is described in figures 25(a) and (b). Figure 25(a) shows the phase-locked average pressure signal and the derived detection boundaries in conjunction with the measured raw pressure signals. In the particular example of figure 25(a), the mean value of the phase-locked data is 0.88 V and lower and upper threshold boundaries are roughly set to 0.75 V and 1.0 V respectively. As shown in figure 25(a), the starting point of the corrupted measurement sequence is detected when the raw pressure signal overshoots the lower threshold limit. In the second step the temperature signal is cross-compared as presented in figure 25(b), and the end of the contaminated sequence is detected when the sensor temperature signal is back to its original average value. This procedure is performed over the entire set of acquired data, the corrupted parts of the measured raw signals are then filtered out and not considered for the following data processing steps, as depicted in figure 24.

9. Uncertainty analysis

In this section, the uncertainties related to flow field measurements in the last stage of low-pressure steam turbine using the FRAP-HTH probe are described. Similar to the work presented by Behr *et al* [23], the whole chain of uncertainty sources has been accounted for. This chain starts with the uncertainties resulting from the calibration references, and the polynomial interpolation curves of the calibration models, as well as the uncertainty sources related to the measurements. The resulting overall uncertainties are calculated by using the

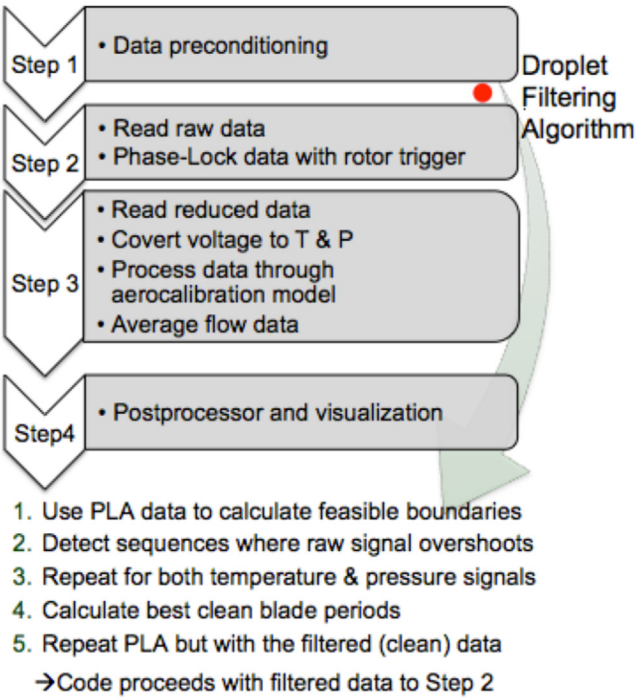

Figure 24. Code structure of Herkules post processing code with the new subroutine implemented between the first and second step of the initial code.

Gaussian error propagation formula. The uncertainty calculation was performed using the guide to the expression of uncertainty in measurement (GUM) [24] which is a commercial workbench for uncertainty calculations.

9.1. Flow angles uncertainties

Figure 26(a) shows the entire chain of uncertainties considered for calculating the uncertainty in measured flow angles accounting for the uncertainties related to calibration and measurement.

According to figure 26(a) the uncertainty calculation for the calibration and measurement procedure involves a number of sources of uncertainties:

1. Pressure DAQ: the overall uncertainty related to the calibration of the piezo-resistive pressure sensors (yaw and pitch sensors calibration) used to measure $p1$–$p6$ pressure taps. This uncertainty is similar during the aerodynamic calibration and the measurements.
2. Probe position and reference flow (calibration): the uncertainty in set flow angles during calibration which depends on the probe installation accuracy on the traversing system and on the traversing system positioning accuracy.
3. Model fit: this uncertainty depends on the quality of the polynomial interpolation curve fit used to model the flow angle calibration coefficients $K\phi$ and $K\gamma$.
4. Probe position (measurement): the uncertainty in set flow angles during measurement which depends on the probe installation accuracy on the traversing system and on the traversing system positioning accuracy.

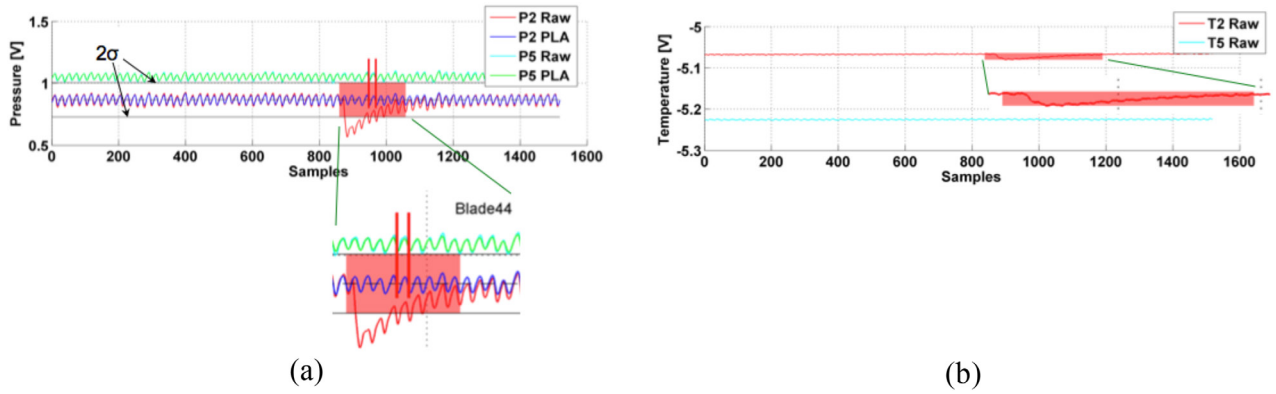

Figure 25. Pressure (a) and temperature (b) signals for the yaw and pitch sensors for 1 rotor revolution. The yaw signal *P*2 is corrupted due to water evaporation.

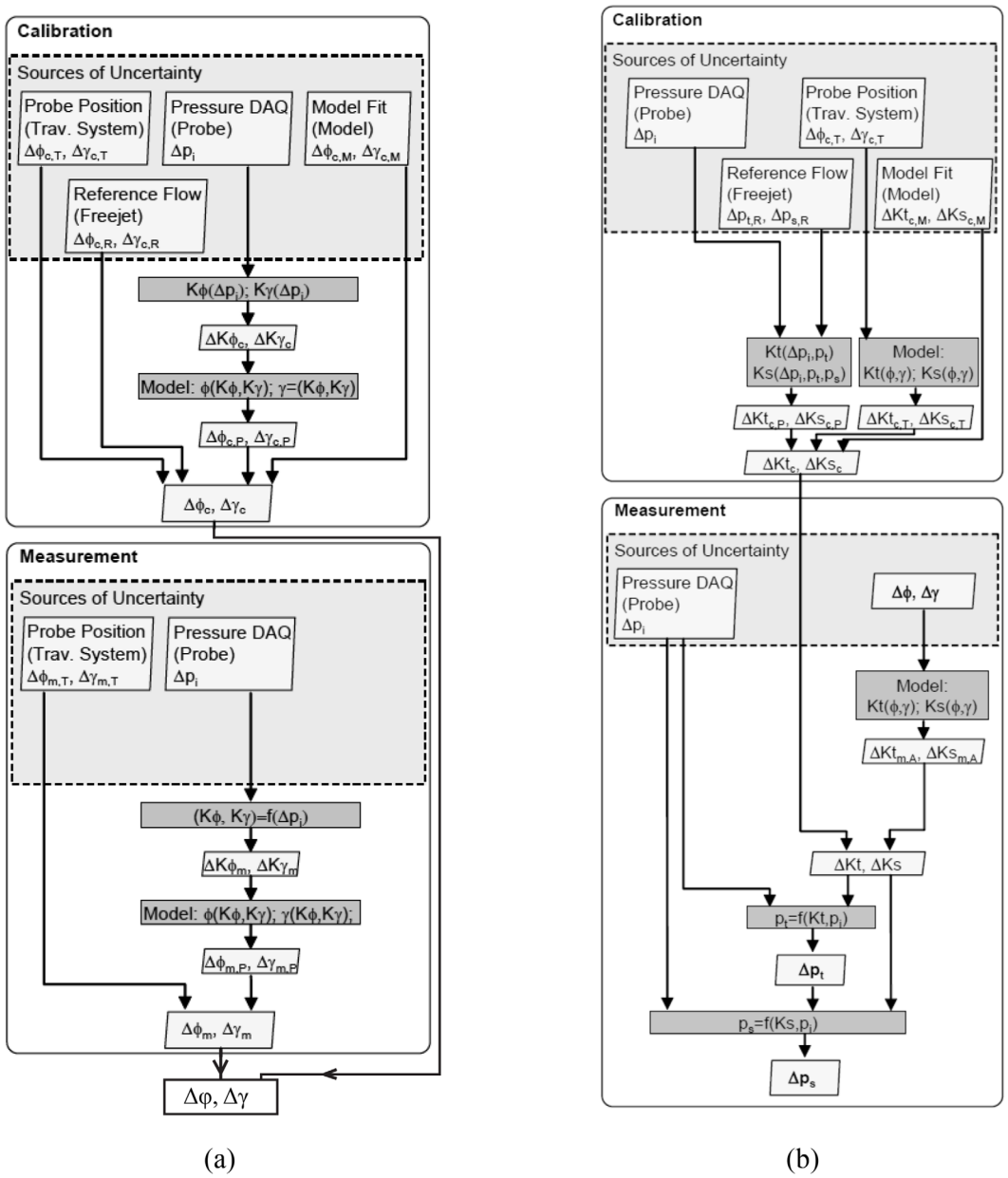

Figure 26. Flow angles' uncertainty propagation (a). Pressure uncertainty propagation of total and static pressure measurement (b).

Table 3. Sources of uncertainty (expanded with coverage factor 2) for the flow angles.

Source of uncertainty		Uncertainty Sector 1	Uncertainty Sector 2	Units
Sensor calibration uncertainties (yaw and pitch sensor)		±25	±25	Pa
Accuracy in probe positioning during aerocalibration	φ	±0.01	±0.01	°
	γ	±0.015	±0.015	
Accuracy in probe positioning during measurements	φ	±0.015	±0.015	°
	γ	±0.015	±0.015	
Pressure data acquisition uncertainty (P_{ref}, P_{atm})		±20	±20	Pa
Model fit uncertainty for aerocalibration	φ	±0.15	0.12	°
	γ	±0.24	0.06	
Reference flow uncertainties during aerocalibration	φ	±0.015	±0.015	°
	γ	±0.015	±0.015	

Table 4. Sources of uncertainty (expanded with coverage factor 2) for the total and static pressure.

Source of uncertainty		Uncertainty Sector 1	Uncertainty Sector 2	Units
Pressure data acquisition uncertainty (P_{ref}, P_{atm})		±20	±20	Pa
Model fit uncertainty for aerocalibration	$\Delta K_{t_{c,T}}$	±0.0019	0.012	
	$\Delta K_{t_{s,T}}$	±0.0084	0.036	

As described in paragraph 4, there are two sets of aerodynamic calibration coefficients which are used to measure over the two pitch and yaw angle incidence range of sector 1 and sector 2 as described in figure 9. All above-mentioned uncertainties for the two sectors are summarized in table 3. The expanded uncertainty resulting from the calibration procedure at Ma = 0.7 is ±0.30° and ±0.49° for the yaw and pitch angle respectively in sector 1 and ±0.14° and ±0.07° for the yaw and pitch angle in sector 2, respectively.

When accounting for the uncertainties during measurements, the overall uncertainty in flow angles measurement is ±0.30° and ±0.49° for the yaw and pitch angles respectively in sector 1 and ±0.20° and ±0.10° in sector 2.

The uncertainty evaluation for the total and static pressure follows the same procedure as described for the flow angles. Figure 26(b) shows a schematic of the uncertainty propagation calculation performed with the GUM workbench for the total and static pressure. The uncertainty calculation uses the same sources of uncertainty as stated in table 3, except for the uncertainties related to the inter polynomial curve fit of the total and static pressure coefficients K_t and K_s which are summarized in table 4.

The overall uncertainties for the two sectors for the measurement conditions found at the nozzle exit of the last stage of a low-pressure steam turbine are presented in table 5. Sector 1 exhibits in general greater values of uncertainties in all flow parameters. The main reason is the higher error arising from the aerodynamic calibration model fit. The calibration coefficient curves for sector 1 are three-dimensional resulting in greater errors on the model fit term as presented in figure 26.

Table 5. FRAP-HTH expanded uncertainty (with coverage factor 2) calculated for L-0 stator exit for Ma = 0.7.

Parameter:	Expanded abs. Uncertainty Sector 1	Expanded abs. Uncertainty Sector 2
φ	±0.30°	±0.20°
γ	±0.49°	±0.10°
P_{tot}	±210 Pa (1.0%P_{tot})	±170 Pa (0.6%P_{tot})
P_{stat}	±480 Pa (2.3%P_{stat})	±390 Pa (1.9%P_{stat})
Ma	±0.032	±0.023
Ma_{rel}	±0.027	±0.017
φ_{rel}	±0.76°	±0.62°
Cpt_{rel}	$\pm 0.6 \times 10^{-3}$	$\pm 0.5 \times 10^{-3}$

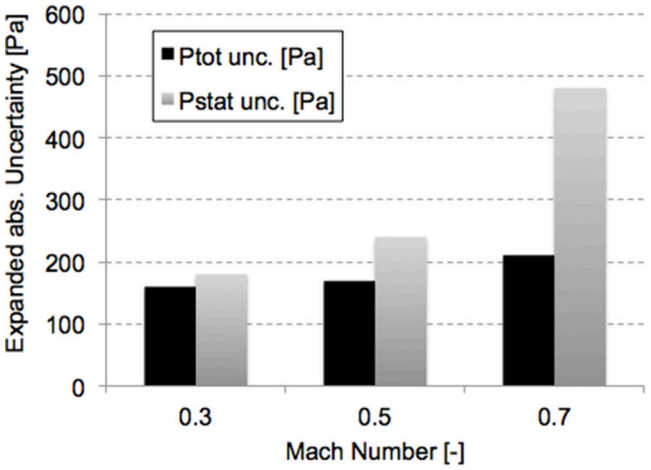

Figure 27. Total and static pressure expanded uncertainties as a function of Mach number.

The total and static pressure uncertainties are 1% and 2.3% of the maximum total and static pressure respectively, which enable accurate measurements in the challenging wet steam environment in the last stage of low pressure steam turbines.

Figure 27 summarizes the uncertainties in measured total and static pressure for Mach number conditions of Ma = 0.3, 0.5 and 0.7. The extended uncertainty of the flow pressures at low Mach numbers at Ma = 0.3 for sector 1 are ±160 Pa for the total pressure and ±180 Pa for the static pressure. In most cases, with increasing Mach numbers the uncertainty of the aerocalibration model increases. The model uncertainty is multiplied with a term representing the partial derivative of the overall uncertainty equation and this term increases as well with higher Mach numbers due to higher absolute pressure levels. As a consequence the model uncertainty contributes more to the overall uncertainty at higher Mach numbers. This effect can be seen in the results shown in figure 27. Nevertheless the relative uncertainties in measured total and static pressure reduce with increased Mach number conditions.

10. Time resolved results from a steam turbine test facility

As mentioned in the introduction section of this paper, the FRAP-HTH probe was used in several measurement campaigns at MHPS research steam turbine test facility [10, 11].

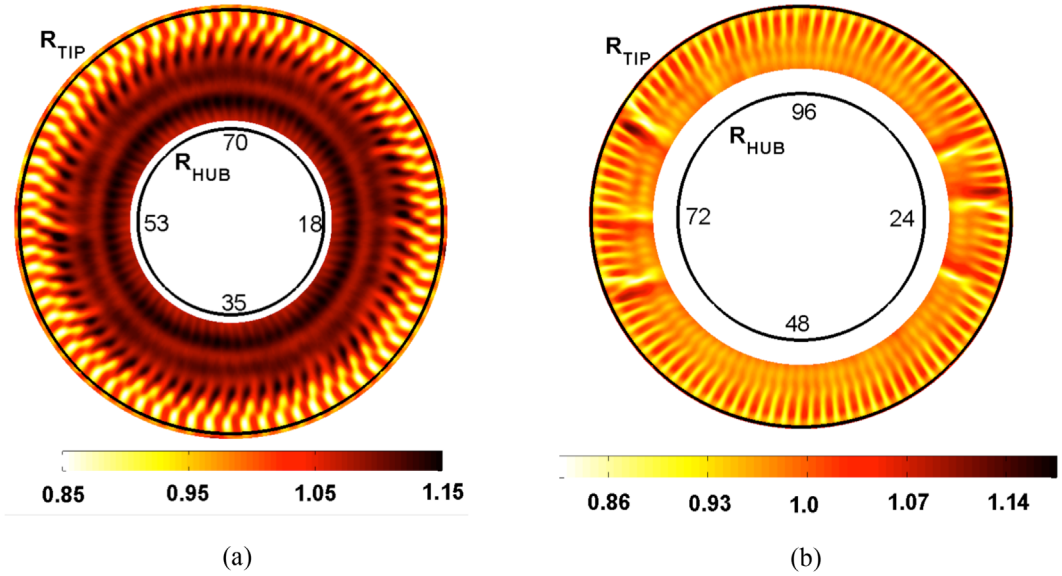

Figure 28. Unsteady total pressure P/P_{avg} obtained from a single traverse at the rotor exit of the L-0 (a) and L-1 (b) planes. The radial axis is the blade span and the azimuthal axis is the blade count over one rotor revolution. The observer looks upstream.

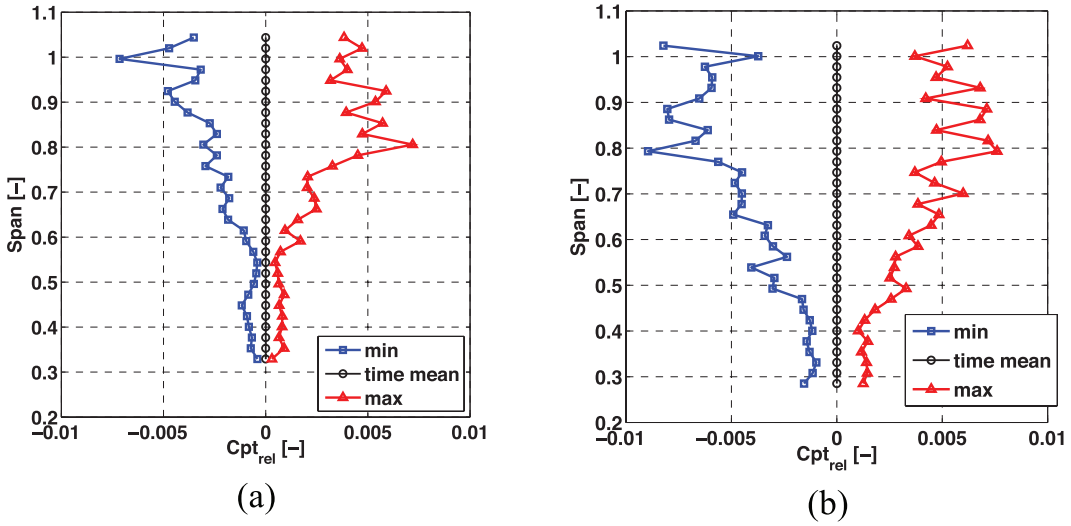

Figure 29. Maximum and minimum deviation from time-averaged mean value of Cpt_{rel} for L-0 (a) and L-1 (b) stage exit.

The new probe was successfully tested in these campaigns and showed the capability to perform time resolved measurements under wet steam conditions.

As presented in [10] the probe was used to perform time resolved measurements at the rotor exit of the last stage (L-0) as well as at the rotor exit of the second to last stage (L-1) of a four stage (L-3 to L-0) low pressure steam turbine. The data were acquired at a sampling rate of 200 kHz over a period of 2 s with a resolution of 24 Bit. The sampling rate resolves 16 points for one rotor blade passage. The probe was mounted on a 2 axis traversing system enabling a single traverse at each measurement plane (L-0 & L-1) from blade hub to blade tip. The spatial resolution of the measurement grid at the traverse planes is 31 and 33 equally distributed radial points for L-0 and L-1 planes respectively. For compactness of this paper the results are focused on the operating point OP-3 as described in [10], with a mass flow of 67*t*/*h*, exit vacuum pressure of 8 kPa and wetness mass fraction of 8.0% for L-0 plane and 3.1% for L-1 plane.

Figures 28(a) and (b) show a space-time diagram of the measured unsteady total pressure downstream of L-0 and L-1 rotor respectively. The radial axis represents the blade span from hub to tip and the circumferential axis the time for one rotor revolution. The number of the blades is plotted as well in the same contour plots. The results have been non-dimensionalized with the mean pressure value measured in the traverse over this one rotor revolution. Besides the modulation in total pressure triggered by the upstream rotor blades, it is worth noting the highly distorted flow field on figure 28(b), around 24 and 72 of the rotor blade passing period. The large fluctuations at the rotor exit of L-1 for those particular blades are induced by the strain gauges attached on the blade surfaces of the steam turbine for blade vibration measurements as described in [12].

Figure 29 shows the minimum and maximum deviation from the time averaged mean value of the relative total pressure coefficient for L-0 and L-1 planes of the experimental

steam turbine test facility. As presented in figure 29, both planes experience the highest Cpt_{rel} variation at the tip with gradually decreasing levels of fluctuations until the hub region. This is due to the higher Euler work extraction, which is dominant at the tip of the blade span and progressively decreases towards the hub. This observation is in good agreement in trend and order of magnitude of the pressure fluctuations with [25]. The mean values of the relative total pressure coefficient at the tip, mid and hub regions are 0.09, 0.05 and 0.04. As a result the unsteady pressure fluctuations relative to the mean value are ±8.5%, ±0.5% and ±0.7% in the tip, mid and hub span locations respectively for the exit of the last stage (L-0) as indicated in figure 29(a). For the exit of L-1 stage the mean values of the Cpt_{rel} are 0.15, 0.13 and 0.11 for the tip, mid and hub regions respectively. In figure 29(b) the unsteady pressure fluctuations relative to the mean value are ±5%, ±2.5% and ±0.9% in the tip, mid and hub span locations respectively.

The current measurements enable, for the first time, an experimental determination and quantification of the unsteady flow field, responsible for the unsteady loading and high cycle fatigue of the rotor blades in the low-pressure stages of an industrial steam turbine. As a consequence, time resolved flow field data are very valuable for the design of the long blades of the LP steam turbines.

11. Conclusions

A new fast response probe for time resolved flow field measurements in wet steam environment was successfully developed and tested in a LP steam turbine test facility. The probe has demonstrated its reliability to perform accurate measurements in severe wet steam conditions with wet-mass fractions up to 8% at the last stages of a steam turbine. The miniature heater, which is used to evaporate the concentrated water in the pressure taps of the probe, has no effect on the measured flow quantities. Test results have shown that the flow quantities, when the heater is activated or deactivated, are within the uncertainty of the aerocalibration model. It mainly affects the total pressure and stagnation pressure coefficient distribution due to its higher blockage effect setting the stagnation condition at 25° of the pitch angle instead of 10° for Mach number of 0.7.

In this paper the detailed calibration procedure is described as well. A new virtual six-sensor measurement concept was applied to capture the high pitch angles of the flow, due to the large flare angles at the last stages of low pressure steam turbines. This has broadened the available operating range of the probe up to roughly 50° in pitch angle instead of 20°. Additionally, shock tube tests in air have provided the transfer function of the new probe and a frequency correction for operation in steam has shown that the probe measurement bandwidth is at 25.3 kHz. The uncertainty analysis was performed with the commercial GUM workbench and the total and static pressure uncertainties are 1% and 2.3% of the maximum total and static pressure respectively, which enable accurate measurements in the challenging wet steam environment. A droplet filtering algorithm to identify corrupted data due to droplet impact or evaporation from the heating process was presented as well.

Last but not least, results at the rotor exit of the last stage from the measurement campaign in MHPS steam turbine test facility are briefly discussed in this paper. Measurements have shown that secondary flow structures at the tip region are the predominant sources of unsteadiness over the last 30% of the blade span for all measurement planes.

Acknowledgments

The authors would like to thank MHPS research group in Hitachi in Japan, for the support as well as for the permission to publish the experimental data. The authors would like in particular to acknowledge, Dr S Senoo for his active contribution and excellent management during the measurement campaigns in Japan. In addition, special thanks go to Mr C Duan and Mr K Ishibashi from MHPS for their active support during the measurement campaigns. Finally the authors thank Mr F Alickaj for his support in the development of the new FRAP-HTH measurement system.

References

[1] Senoo S and Ono H 2013 Development of design method for supersonic turbine aerofoils near the tip of long blades in steam turbines part 2: configuration details and validation *Oil and Gas Applications* vol 5B (San Antonio: Steam Turbines) GT2013-94039

[2] Haraguchi M, Nakamura T, Yoda H, Kudo T and Senoo S 2013 Nuclear steam turbine with 60 inch last stage blade *Proc. ASME 55782 Plant Operations, Maintenance, Engineering, Modifications, Life Cycle and Balance of Plant; Nuclear Fuel and Materials; Radiation Protection and Nuclear Technology Applications* vol 1 ICONE21-16600

[3] Shibukawa N, Iwasaki Y, Takada Y, Murakami I, Suzuki T and Fukushima T 2014 *An Experimental Investigation of the Influence of Flash-Back Flow on Last Three Stages of Low Pressure Steam Turbines* vol 1B (Düsseldorf: ASME) GT2014-26897

[4] Cai X *et al* 2014 Coarse water in low-pressure steam turbines *Proc. Inst. Mech. Eng.* A **228** 153–67

[5] Sigg R, Casey M V, Mayer J F and Sürken N 2008 The influence of lean and sweep in a low pressure steam turbine: analysis of three stages with a 3D CFD model *Turbomachinery* vol 6 (Berlin: ASME) GT2008-50161

[6] Häfele M *et al* 2014 Numerical investigation of the impact of part-span connectors on aero-thermodynamics in a low pressure industrial steam turbine *Marine; Microturbines, Turbochargers and Small Turbomachines; Steam Turbines* vol 1B (Düsseldorf: ASME) GT2014-25177

[7] Völker L, Casey M, Dunham J and Stüer H 2008 The influence of lean and sweep in a low pressure steam turbine: throughflow modelling and experimental measurements *Turbomachinery* vol 6 (Berlin: ASME) GT2008-50161

[8] Segawa K, Senoo S, Kudo T, Nakamura T and Shibashita N 2012 Steady and unsteady flow measurements under low load conditions in a low pressure model steam turbine *Thermal-Hydraulics; Turbines, Generators, and Auxiliaries* vol 3 (Anaheim: ASME) ICONE20-POWER2012-54862

[9] Gerschütz W, Casey M and Truckenmüller F 2005 Experimental investigations of rotating flow instabilities in the last stage of a low-pressure model steam turbine during windage *Proc. Inst. Mech. Eng.* A **219** 499–510

[10] Bosdas I, Mansour M, Kalfas A I, Abhari R S and Senoo S 2015 Unsteady wet steam flow field measurements in the last stage of low pressure steam turbine *J. Eng. Gas Turbines Power* **138** 032601
[11] Bosdas I, Mansour M, Kalfas A, Abhari R and Senoo S 2015 Unsteady wet steam flow field and droplet measurements at the last stage of low-pressure steam turbine *Presented at the IGTC (Tokyo, Japan, 2015)*
[12] Duan C *et al* 2015 Unsteady wet steam flow measurements in a low-pressure test steam turbine *Presented at the 13th Asian Int. Conf. on Fluid Machinery (Tokyo, Japan, September 2015)*
[13] Kuperfschmied P, Köppel P, Roduner C and Gyarmathy G 2000 On the development and application of The FRAP (fast-response aerodynamic probe) system for turbomachines—part 1: the measurement system *J. Turbomach.* **122** 505–16
[14] Pfau A, Schlienger J, Kalfas A I and Abhari R S 2002 Virtual four sensor fast response aerodynamic probe (FRAP) *16th Symp. on Measuring Techniques in Transonic and Supersonic Flow in Cascades and Turbomachines (Cambridge, UK)*
[15] Mansour M, Chokani N, Kalfas A I and Abhari R S 2008 Time-resolved entropy measurements using a fast response entropy probe *Meas. Sci. Technol.* **19** 115401
[16] Lenherr C, Kalfas A I and Abhari R S 2010 High temperature fast response aerodynamic probe *J. Eng. Gas Turbines Power* **133** 011603–13
[17] Mansour M, Kocer G, Lenherr C, Chokani N and Abhari R S 2011 Seven-sensor fast-response probe for full-scale wind turbine flowfield measurements *J. Eng. Gas Turbines Power* **133** 081601
[18] Gossweiler C R, Kupferschmied P and Gyarmathy G 1995 On fast-response probes: part 1—technology, calibration, and application to turbomachinery *J. Turbomach.* **117** 611–7
[19] Gallington R W 1980 Measurement of very large flow angles with non-nulling seven-hole probe *Aeronaut. Dig.* 60–80 USAFA-TR-80-17
[20] Bohn D and Simon H 1975 Mehrparametrige Approximation der Eichraeume und Eichflaechen von Unterschall- und Ueberschall-5-Loch-Sonden *Tech. Mess.—ATM* 468–79
[21] Li C, Wang X, Cheng D and Sun B 2008 Experimental study on effects of slot hot blowing on secondary water droplet size and water film thickness *J. Eng. Gas Turbines Power* **131** 033001
[22] Schlienger J 2003 Evolution of unsteady secondary flow in a multistage schrouded axial turibne *PhD Thesis* ETH, Zurich ETH Nr 15230
[23] Behr T, Anestis I K and Abhari R 2006 A probabilistic uncertainty evaluation method for turbomachinery probe measurements *XVII Symp. on Measuring Techniques in Turbomachinery. Transonic and Supersonic Flow in Cascades and Turbomachines (Thessaloniki Greece, 21–22 September 2006)*
[24] ISO 1995 *Guide to the Expression of Uncertainty in Measurement (GUM)* (International Organisation for Standardisation)
[25] Qi M, Yang J, Yang R and Yang H 2013 Investigation on loading pulsation of LP long blade stage in steam turbine *Oil and Gas Applications; Steam Turbines* vol 5B (San Antonio: ASME) GT2013-94652